Baghdad Science Journal

Volume 23 | Issue 4 Article 2

4-20-2026

Study the Effect of Isospin Dependence and Short-Range Correlations by Using Contact Formalism through Inclusive Nuclear Structure for ^{20}Ne and ^{24}Mg Nuclei

Farah Faris Kaddoori
Department of Physics, College of Science, University of Baghdad, Baghdad, Iraq AND Department of Physics, College of Science for Women, University of Baghdad, Baghdad, Iraq,
farahfaris@csw.uobaghdad.edu.iq

Ghaith N. Flaiyh
Department of Physics, College of Science, University of Baghdad, Baghdad, Iraq,
ghaith.flaiyh@sc.uobaghdad.edu.iq

How to Cite this Article

Kaddoori, Farah Faris and Flaiyh, Ghaith N. (2026) "Study the Effect of Isospin Dependence and Short-Range Correlations by Using Contact Formalism through Inclusive Nuclear Structure for ^{20}Ne and ^{24}Mg Nuclei," *Baghdad Science Journal*: Vol. 23: Iss. 4, Article 2.
DOI: https://doi.org/10.21123/2411-7986.5256

BAGHDAD SCIENCE JOURNAL 2026;23(4):1125–1134

RESEARCH ARTICLE

Study the Effect of Isospin Dependence and Short-Range Correlations by Using Contact Formalism through Inclusive Nuclear Structure for ^{20}Ne and ^{24}Mg Nuclei

Farah Faris Kaddoori [1,2,*], **Ghaith N. Flaiyh** [1]

[1] Department of Physics, College of Science, University of Baghdad, Baghdad, Iraq
[2] Department of Physics, College of Science for Women, University of Baghdad, Baghdad, Iraq

ABSTRACT

Pair densities and their related correlation functions play a crucial role in capturing the complex many-body interactions within nuclear systems. This study focuses on how spin and isospin specifically influence nuclear charge density distributions. Using the folding model, the charge density is derived through an effective two-body density approach that incorporates both short-range correlations (SRC's) and tensor correlations (TC's), while also accounting for spin- and isospin-dependent forces. Calculations were carried out for the elastic electron scattering form factors, $F(q)$, and the root-mean-square (RMS) charge radii, $\langle r^2\rangle^{1/2}$, of the ^{20}Ne and ^{24}Mg nuclei. The study also examined inelastic longitudinal electron scattering form factors for isoscalar transitions (T = 0) from the ground state to the excited states ($0^+0 \rightarrow 2^+0$) and ($0^+0 \rightarrow 4^+0$) in the same nuclei. These analyses incorporated core polarization effects using the Tassie model. The results closely matched experimental observations, underscoring the reliability and precision of the theoretical approach used.

Keywords: Charge density distribution (CDD), Core polarization effects, Form factor (FF's), Short range correlation (SR'C), Tensor correlations (TC's)

Introduction

The atomic nucleus stands as one of the most intricate quanta many-body systems in nature, with its internal structure shaped by short-range correlations (SRC's) driven by strong, close-range interactions between nucleons. These correlations leave a noticeable imprint on the charge density distribution, $\rho_{ch}(r)$, a key observable that reflects the nucleus's size, shape, and internal dynamics. SRCs tend to shift nucleons from the central region toward the surface, leading to a reduction in central density and an enhancement of the outer regions. This redistribution significantly influences both the root-mean-square (RMS) charge radius, $\langle r^2\rangle^{1/2}$, and the overall stiffness of the nucleus.[1] The isospin dependence of short-range correlations (SRC's) adds another layer of complexity to our understanding of nuclear structure. Both experimental data and *ab initio* calculations have shown a clear dominance of neutron-proton (np) pairs over proton-proton (pp) or neutron-neutron (nn) pairs in high-momentum correlated states. This preference is primarily driven by the tensor component of the nucleon-nucleon (NN) interaction, which is significantly stronger in np pairs because they can form spin-triplet states.[2] Supporting this, recent inclusive electron scattering experiments on calcium isotopes—such as the comparison between ^{48}Ca

Received 3 May 2025; revised 13 June 2025; accepted 3 July 2025.
Available online 20 April 2026

* Corresponding author.
E-mail addresses: farahfaris@csw.uobaghdad.edu.iq (F. F. Kaddoori), ghaith.flaiyh@sc.uobaghdad.edu.iq (G. N. Flaiyh).

https://doi.org/10.21123/2411-7986.5256

and ^{40}Ca have provided evidence of this isospin dependence, with cross-section ratios aligning with the expected np-pair dominance at momenta beyond the Fermi level.[3] These insights highlight the importance of incorporating both short-range correlations (SRC's) and isospin effects into nuclear models to accurately capture and interpret experimental observables. One effective way to quantify these correlations is through nuclear correlation functions, $O_{NN}(r)$, which are defined as the ratio between correlated and uncorrelated two-body densities. These functions reveal how nuclear systems deviate from mean-field behavior, especially at short distances (typically $r \lesssim 1$ fm).[4] Recent studies have investigated the role of short-range correlations (SRCs) and tensor correlations (TCs) in shaping nuclear charge distributions and electron scattering observables. Cruz-Torres et al.[5] and Weiss et al.[6] explored the isospin dependence of SRCs in light nuclei using ab initio frameworks. Hamoudi and Abbas[7] applied short-range correlations to electron scattering in fp- and N50-shell nuclei, achieving improved agreement with experimental form factors. In addition, Flaiyh and Sharrad[8] studied the impact of core polarization and two-body correlations on inelastic C2 form factors for ^{10}B. Building upon these foundations, the present work introduces a new blended correlation function. It applies it to both elastic and inelastic electron scattering in ^{20}Ne and ^{24}Mg, providing enhanced insight into the interplay among SRC, TC, and nuclear-structure effects. In this context, the "contact formalism"[5] has become a valuable framework, allowing researchers to separate universal short-range nuclear dynamics—represented by contact coefficients $C_A^{NN,s}$ from long-range, nucleus-specific structure. For example, in ^{40}Ca, the density of neutron-proton (np) spin-1 pairs reaches a peak of 0.8 fm^{-3}, which is roughly four times higher than that of proton-proton (pp) pairs.[9] These characteristics play a crucial role in analyzing electron scattering experiments, particularly at high momentum transfers ($Q_2 \geq 1.5$ GeV^2/c^2), where the dynamics are largely governed by short-range correlations (SRC's).[10] Here, we establish a solid mathematical framework to study nuclear structure in a way that includes short-range correlations (SRC's) and tensor correlations (TC's) in the contact formalism. The use of this formalism enables us to calculate the charge density distributions of ^{20}Ne and ^{24}Mg, which are then used to derive the form factors for elastic and inelastic electron scattering. Our formalism differs from other studies that employ phenomenological or mixed-theory treatments in that we derive all of our observables—from ground-state densities to scattering responses—consistently in the contact formalism. For quantitative precision, we build two-body correlation density distributions (2BCDD's) based on harmonic oscillator wave functions, scaled to experimental RMS radii. This approach captures not only the leading role of SRC's and isospin dependence in nuclear structure but also relates universal short-range dynamics to nucleus-dependent characteristics in a direct manner. By bringing together descriptions of both static densities and dynamical scattering processes in a uniform theory, we offer a predictive and experimentally tested model that improves the accuracy of ab initio-inspired calculations in nuclear physics.

Theory

The operator $\hat{\rho}^{(1)}(\vec{r})$ in Eq. (1) is utilized to express the nucleon density of a nucleus composed of A point-such as particles[11]:

$$\hat{\rho}^{(1)}\left(\vec{r}\right) = \sum_{i=1}^{A} \delta\left(\vec{r} - \vec{r}_i\right) \tag{1}$$

Where $\delta(\vec{r} - \vec{r}_i)$ is the Dirac delta function

To convert this operator for a two-body density taken as[11]:

$$\sum_{i=1}^{A} \delta(\vec{r} - \vec{r}_i) \equiv \frac{1}{2(A-1)} \sum_{i \neq j} \left\{ \delta(\vec{r} - \vec{r}_i) + \delta(\vec{r} - \vec{r}_j) \right\} \tag{2}$$

To represent the charge distribution and nucleon interactions within a nucleus, we begin by considering the two-body structure of the nucleon density operator. This formulation accounts for both the internal structure of the nucleus and nucleon–nucleon interactions. Using the two-body density operator defined below, the charge distribution—modified by electromagnetic interactions—can be expressed as[11]:

$$\hat{\rho}^{(2)}(\vec{r}) = \frac{\sqrt{2}}{(A-1)} \sum_{i \neq j} \left\{ \delta\left[\sqrt{2}\vec{r} - \vec{R}_{ij} - \vec{r}_{ij}\right] + \delta\left[\sqrt{2}\vec{r} - \vec{R}_{ij} + \vec{r}_{ij}\right] \right\} \tag{3}$$

Where is the relative $\vec{r}_{ij}$ and center – of – mass $\vec{R}_{ij}$ coordinates

Through folding the two-body correlation functions using an operator from Eq. (3), it could be possible to develop an effective two-body density of charge operators (such as usage with uncorrelated wave functions). $\tilde{O}_{ij}$ which is correlation operator

(SRC + tensor).[11]

$$\hat{\rho}^{(2)}_{\text{eff}}(\vec{r}) = \frac{\sqrt{2}}{2(A-1)} \sum_{i \neq j} \tilde{O}_{ij} \Big\{ \delta\big[\sqrt{2}\vec{r} - \vec{R}_{ij} - \vec{r}_{ij}\big] + \delta\big[\sqrt{2}\vec{r} - \vec{R}_{ij} + \vec{r}_{ij}\big] \Big\} \tilde{O}_{ij} \quad (4)$$

the form of $\tilde{O}_{ij}$ is provided by[5]

$$\tilde{O}_{ij} = O\left(r_{ij}\right) \nabla_1 + O\left(r_{ij}\right) \left\{1 + \beta\left(\mathrm{A}\right) S_{ij}\right\} \nabla_2 \quad (5)$$

Where β(A) is the tensor correlation strength β(A).

It is evident that Eq. (5) incorporates two distinct types of correlations. The first term, $O(r_{ij})$, represents short-range correlations between two nucleons, while ∇_1 functions as a projection operator onto the space of two-body wave functions. At short distances—where particles are repelled by the strong short-range core—these correlations reduce the two-body wave function, playing a critical role in particle-pair separation. As the interparticle distance increases and the interaction weakens, $O(r_{ij})$, gradually approaches unity. A basic model for $O(r_{ij})$ It is described in.[10]

$$O\left(r_{ij}\right) = g_{NN}\left(r\right) C^{s}_{NN} + \kappa\left(1 - g_{NN}\left(r\right)\right) \quad (6)$$

To account for nuclear behavior up to $r \leq 0.9$ fm, we propose a model that combines the correlated density derived from the nuclear contact formalism with a longer-range component that applies where correlations become less significant. Using the specified function $g_{NN}(r)$, the correlation function $O(r_{ij})$ is defined as a combination of these two components.

$g_{NN}(r)\, C^{s}_{NN}$ represents the short-range contribution, in which:

Modeling the behavior of nucleon pairs under short-range correlations (SRC's), the correlation function $g_{NN}(r)$ is set to unity for $r \leq 0.9$ fm, representing the region dominated by SRC's. An example of this framework includes evaluating the probability of finding correlated nucleon pairs, denoted by the contact coefficient. C^{s}_{NN}. Using the relation provided in Ref.[10], the contact coefficient for proton–proton pairs, C^{s}_{PP}, is computed by.[6]

$$C^{0}_{PP} = \mathrm{b}W^2 \,/\, A \quad (7)$$

In which the b-size harmonic oscillator parameter was applied, and Eq. (8) was used to predict W[6]:

$$W \approx \frac{A}{2}\left[1 - \frac{a_c A^{2/3}}{4a_A}\right] \approx \frac{A}{2}\left[1 - 0.0075A^{2/3}\right] \quad (8)$$

About 0.711 MeV and 23.7 MeV, respectively, are the coefficients of the Coulomb. a_c and Asymmetry a_A components in the mass equation.

At distances (r > 0.9), the two-body correlations function $g_{NN}(r)$ gradually transitions to account for the uncorrelated density's behaviour. The definition of $g_{NN}(r)$ in the suggested framework, it is as follows[10]:

$$g_{NN(r)} = \begin{cases} 1 & (r \leq 0.9\mathrm{fm}) \\ \frac{1}{k}\left(k - 1 + e^{(0.9fm - r)/a)}\right) & (r > 0.9\mathrm{fm}) \end{cases} \quad (9)$$

The model describing two-body densities and correlation functions in nuclear systems relies significantly on the parameters κ and α. In this context, κ governs the transition length scale between short-range and long-range regimes, while α determines the long-range asymptotic behavior, ensuring that the correlation function. $g_{NN(r)}$ approaches $(\kappa - 1)/\kappa$ as $r \to \infty$. Both κ and α are influenced by isospin and the type of nucleus, reflecting variations in the interaction strength among proton–proton (pp), neutron–neutron (nn), and proton–neutron (pn) pairings. As a result, long-range correlation behavior becomes increasingly sensitive to isospin.[6]

The second term in Eq. (5) represents two-body tensor correlations, which extend over a longer range and arise from the strong tensor component of the nucleon–nucleon interaction. In this context, ∇_2 denotes a gradient operator acting only on the $^3S_1$ and $^3D_1$ states. The tensor operator S_{ij}, as described in,[7,12] is a standard second-rank operator in coordinate space, coupled to the internal spin structure and multiplied by a scalar quantity to ensure proper transformation under rotations given by Eq. (10).[7] Where: S_{ij} is a tenser force, $(\vec{\sigma}_i.\vec{\sigma}_j)$ is the scalar product of the Pauli spin matrices for nucleons i and j, representing their spin-spin interaction, $\vec{\sigma}_i.\vec{r}_{ij}$ scalar product between the spin of nucleon i and its relative position vector $\vec{r}_{ij}$ and $(\vec{\sigma}_j.\vec{r}_{ij})$ scalar product between the spin of nucleon j and the relative position vector $\vec{r}_{ij}$.

$$S_{ij} = \frac{3}{r^2_{ij}}\left(\vec{\sigma}_i.\vec{r}_{ij}\right).\left(\vec{\sigma}_j.\vec{r}_{ij}\right) - \vec{\sigma}_i.\vec{\sigma}_j \quad (10)$$

The tensor correlation strength, shown by the parameter β(A) in Eq. (5), is not zero in both of the $^3S_1$ and $^3D_1$ channels.

In Eq. (4), the expected value of the efficient operator for two-body charge density yields the ground state distribution of two-body charge densities. $\rho_{ch}(r)$, which may be written as 12

$$\langle\Psi|\,\hat{\rho}^{(2)}_{eff}\left(\vec{r}\right)|\Psi\rangle = \sum_{i<j}\langle ij|\,\hat{\rho}^{(2)}_{eff}\left(\vec{r}\right)\big[|ij\rangle - |ji\rangle\big] \quad (11)$$

where $|ij\rangle$ is the two-particle wave function.

The definition for (the radius of the nuclear root mean square charge $\langle r^2\rangle^{1/2}$ equal to.[13]

$$\langle r^2\rangle^{1/2} = \frac{4\pi}{Z}\int_0^\infty \rho_{ch}(r) r^4\, dr \tag{12}$$

For spin-zero nuclei, the two-body charge density distribution in the ground state, $\rho_{ch}(r)$, as defined in Eq. (11), is associated with the elastic electron scattering form factor. The form factor is simply the Fourier transform of $\rho_{ch}(r)$.[8]

$$F(q) = \frac{4\pi}{qZ}\int_0^\infty \rho_o(r)\sin(qr) r\, dr \tag{13}$$

In the case of inelastic electron scattering, longitudinal or Coulomb scattering is an effect of the electron's interaction via the nucleus's charge distribution, with the multipole operators' matrix components $\hat{T}_J^L\ (q)$, the longitudinal shape factors relate to the charge density distributions (CDD).[14]

$$|F_J^L(q)|^2 = \frac{4\pi}{Z^2(2J_i+1)}|\langle f||\hat{T}_J^L(q)||i\rangle|^2 |F_{cm}(q)|^2 |F_{fs}(q)|^2 \tag{14}$$

When using the shell model wave function, the center-of-mass correction eliminates the spurious state caused by the mobility of the center of mass, $F_{cm}(q)$, where Z, the atomic number of the nucleus, is given as.[15]

$$F_{cm}\,(q) = e^{q^2.b^2/4A} \tag{15}$$

Here, b is the harmonic oscillator size parameter, and A denotes the mass number, assumed to be the same for protons and neutrons. The independent nucleon form factor is represented by the function $F_{fs}(q)$, which takes the form.[15]

$$F_{fs}\,(q) = e^{-0.43.q^2/4} \tag{16}$$

The definition of the longitudinal operator is.[16]

$$\hat{T}^L_{J_{t_z}}(q) = \int_0^\infty dr\, j_J(qr) Y_J(\Omega)\rho(r, t_z) \tag{17}$$

The spherical harmonic wave structure is represented by $Y_J(\Omega)$, while the charge density operator is denoted by $\rho(r, t_z)$, and $j_J(qr)$ is the spherical Bessel function. The reduced matrix elements $\hat{T}^L_{JT}$ between the system's initial and final multi-particle states can be expressed in both spin and isospin space using one-body density matrix (OBDM) components, multiplied by the single-particle matrix elements of the longitudinal operator, which involve configuration mixing,[17] i.e.,

$$\langle f|||\hat{T}^L_{JT}|||i\rangle = \sum_{a,b} OBDM^{JT}(i, f, J, a, b)\langle b|||\hat{T}^L_{JT}|||a\rangle \tag{18}$$

Where
i: Initial many-body nuclear state
f: Final many-body nuclear state
J: Total angular momentum of the nuclear transition
a: Single-particle quantum state in the initial configuration
b: Single-particle quantum state in the final configuration

The many-particle reduced matrix elements of the longitudinal operator consist of two parts; one is for the model space $\overset{m\ s}{\hat{T}}{}^L_J\ (\tau_Z, q)$ and the other is for the core polarization matrix element $\overset{core}{\hat{T}}{}^L_J\ (\tau_Z, q)$.[8]

$$\langle f\|\hat{T}^L_J(\tau_Z, q)\|i\rangle = \langle f\|\hat{T}^{L,ms}_J(\tau_Z, q)\|i\rangle + \langle f\|\hat{T}^{L,core}_J(\tau_Z, q)\|i\rangle \tag{19}$$

In Eq. (19), the model space matrix element takes the following form[17]:

$$\left\langle f\left\|\overset{ms}{\hat{T}}{}^L_J(\tau_Z, q)\right\|i\right\rangle = e_i\int_0^\infty drr^2 j_J(qr)\overset{ms}{\rho}{}_{J,\tau_Z}(i, f, r) \tag{20}$$

Here, ei represents the effective charge of the nucleon involved in the transition between initial (i) and final (f) states and $\overset{ms}{\rho}{}_{J,\tau_Z}$ is the transition density of charges for the model space, and is supplied by[17]

$$\rho^{ms}_{J,\tau_Z}(i, f, r) = \sum_{jj'(ms)}^{ms} OBDM(i, f, J, j, j', \tau_z) \times \langle j\|Y_J\|j'\rangle R_{nl}(r)R_{\dot{n}\dot{l}}(r) \tag{21}$$

The element of the core polarization matrix is provided by[17]

$$\left\langle f\left\|\overset{core}{\hat{T}}{}^L_J(\tau_Z, q)\right\|i\right\rangle = e_i\int_0^\infty drr^2 j_J(qr)\overset{core}{\rho}{}_J(i, f, r) \tag{22}$$

The transition density of core polarization, denoted as $\overset{core}{\rho}{}_J$, depends on the core polarization model. To account for core polarization effects, the transition density associated with the model space is supplemented by the core polarization transition density, which is used to describe all excitation modes within the nucleus. The resulting total transition density is

Table 1. Given the open-shell nuclei' ground state 2BCDD properties.

Nuclei	b	β (A)	k(A)	α(A)	$\eta_{1s_{\frac{1}{2}}}$	$\eta_{1p_{\frac{3}{2}}}$	$\eta_{1p_{\frac{1}{2}}}$	$\eta_{1d_{\frac{5}{2}}}$	$\eta_{2s_{\frac{1}{2}}}$	$\eta_{1d_{\frac{3}{2}}}$	$\eta_{2p_{\frac{3}{2}}}$
^{20}Ne	1.9	0.085	9.0	0.7	1	1	1	0.083	0.25	0.25	–
^{24}Mg	1.96	0.084	6.0	0.55	1	1	1	0.333	–	0.25	0.25

Table 2. Root-Mean-Square (RMS) charge radii.

Nuclei	$\langle r^2\rangle^{1/2}_{with\ out.}$	$\langle r^2\rangle^{1/2}_{with\ corr.}$	$\langle r^2\rangle^{1/2}_{\text{exp.}}$ [18,19]
^{20}Ne	2.722	2.864	3.006 ± 0.015
^{24}Mg	2.763	2.967	3.057 ± 0.020

given by.[17]

$$\rho_{J,\tau_Z}(i,f,r) = \overset{ms}{\rho}_{J,\tau_Z}(i,f,r) + \overset{core}{\rho}_{J,\tau_Z}(i.f.r) \quad (23)$$

Based on the combined modes of the nucleus, the Tassie form defines the core polarization transition density.[8]

$$\rho^{core}_{Jt_z}(i,f,r) = N\frac{1}{2}(1+\tau_z)r^{J-1}\frac{d\rho_o(i,f,r)}{dr} \quad (24)$$

which represents the base state two-body charge density distribution ρ_o, as expressed in Eq. (4) and including a propagator constant N, the Coulomb form factor $F^L_J(q)$ is.[8]

$$F^L_J(q) = \sqrt{\frac{4\pi}{2J_i+1}}\frac{1}{Z}\left\{\int_0^\infty r^2 j_J(qr)\rho^{ms}_J(i,f,r)\,dr + N\int_0^\infty dr r^2 j_J(qr)r^{J-1}\frac{d\rho_o(i,f,r)}{dr}\right\}F_{cm}(q)F_{fs}(q) \quad (25)$$

The proportionality constant N is obtained as follows[8]:

$$N = \frac{\int_0^\infty dr r^2 j_J(kr)\rho^{ms}_{Jt_z}(i,f,r) - \sqrt{\frac{(2J_i+1)B(CJ)}{(2J+1)!!}}k^J}{k\int_0^\infty dr r^{J+1}\rho_o(i,f,r)j_{J-1}(kr)} \quad (26)$$

Here,
k: Magnitude of the momentum transfer in the inelastic electron scattering process.
kr: Dimensionless product of the momentum transfer k and radial coordinate r, appearing as an argument in the spherical Bessel function $j_J(kr)$.
k^J: Momentum transfer raised to the power J, corresponding to the multipole order of the transition. And B(CJ): is a reduced transition probability.

Results and discussion

For the ^{20}Ne and ^{24}Mg nuclei, calculations have been performed for the ground-state two-body charge density distributions (2BCDD's), $\rho_{ch}(r)$, the root-mean-square (RMS) charge radii $\langle r^2\rangle^{1/2}$, and both elastic and inelastic electron scattering form factors, $F(q)$'s. The higher-lying single-particle states $1d_{5/2}$ and $2s_{1/2}$ are included in the model space for these nuclei. The occupation probabilities of these higher states are presented in Table 1. The strength of the correlations is determined by comparing the calculated $\langle r^2\rangle^{1/2}$ values with experimental data. Table 1 and Table 2 summarize all parameters used in the computation of $\rho_{ch}(r)$, $\langle r^2\rangle^{1/2}$, and $F(q)$'s, including the oscillator size parameter (b), the tensor correlation strength $\beta(A)$, the correlation range parameter $k(A)$, the exponential decay length $\alpha(A)$, and the occupation probabilities η_s of the relevant states.

The two-body charge density distributions, ρ_{ch}(r), are presented in Fig. 1—specifically, Fig. 1(a) for ^{20}Ne and Fig. 1(b) for ^{24}Mg—in three representations. The solid curve includes both short-range correlations (SRC's) and tensor correlations (TC's), calculated from Eq. (4); the dashed curve represents results without correlations, based on Eq. (1); and the discrete points or dotted line correspond to fitted experimental data.[18,19] In the absence of correlations, the dashed curve reflects the naive assumption of noninteracting nucleons and deviates significantly from experimental data, particularly at small r values. By including SRC's and TC's, as illustrated by the solid curve, protons are redistributed from the central to the surface regions, thereby reducing the central peak and slightly enhancing the tail of the distribution. The improved agreement between theoretical predictions and experimental data underscores the crucial role of spin- and isospin-dependent nucleon-nucleon interactions in accurately modeling nuclear charge densities.

The elastic electron scattering form factors, F(q), for the ^{20}Ne and ^{24}Mg nuclei exhibit oscillatory behavior due to interference among electronically scattered waves, reflecting the spatial distribution of nucleons within the nucleus. Eq. (14) is computed using the ground-state two-body charge density distributions obtained from Eq. (11). Fig. 2—specifically, Fig. 2(a) for ^{20}Ne and Fig. 2(b) for ^{24}Mg—compares the calculated $F(q)$'s values with experimental data.[20] The experimental results are represented by dotted symbols, while the calculated $F(q)$'s curves—with

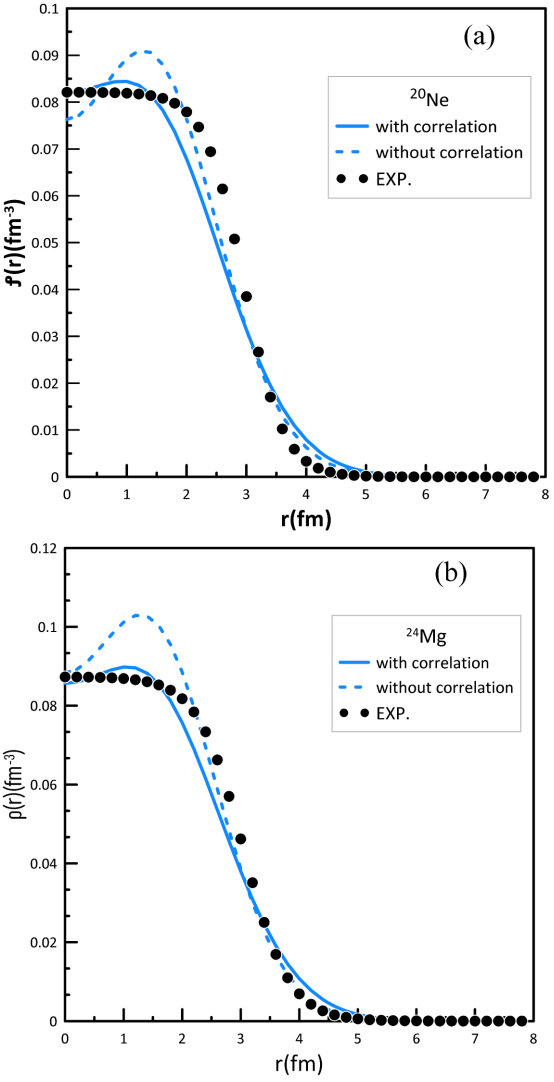

Fig. 1. charge density reliance on r(fm) for the ^{20}Ne (Fig. a) and ^{24}Mg (Fig. b) nuclei. The experimental data of [18,19] are represented by the dotted symbols.

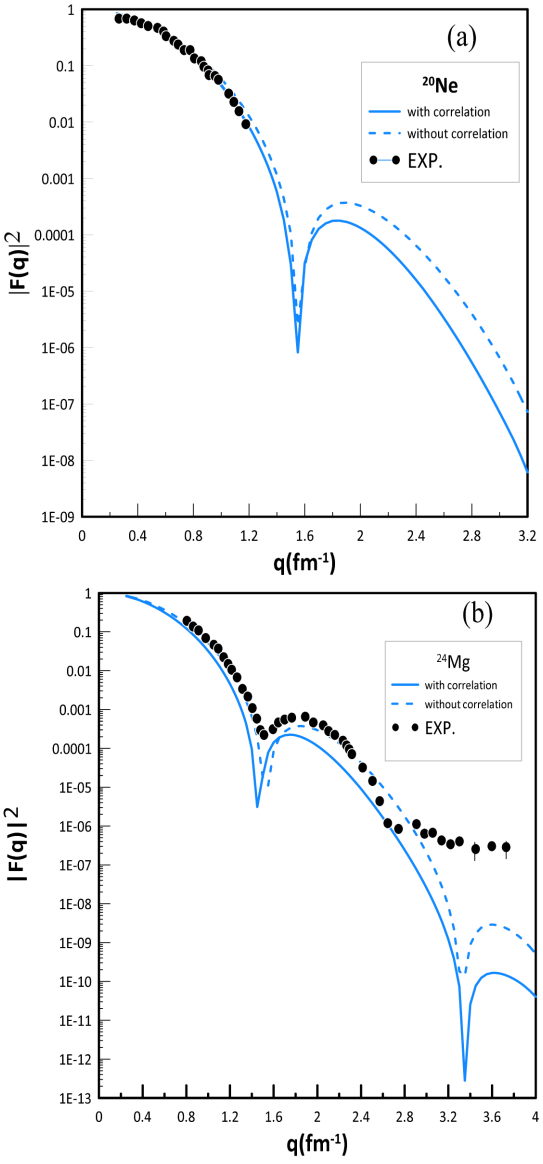

Fig. 2. Elastic Form Factor for ^{20}Ne (Fig. a) and ^{24}Mg (Fig b) nuclei. The filled circle marks are experimental data.[21,22]

and without the inclusion of short-range correlations (SRC's) and tensor correlations (TC's)—are shown as solid and dashed lines, respectively. For ^{20}Ne, the available experimental measurements[20] are confined to a narrow momentum transfer range ($q < 1.2$ fm^{-1}). Within this range, the solid and dashed curves, representing the theoretical predictions, agree reasonably well with the experimental data. For the ^{24}Mg nucleus, both the solid and dashed curves reconstruct the first diffraction minimum observed in the experimental results[20] with satisfactory accuracy. Overall, the calculated $F(q)$'s values show good agreement with experimental observations up to $q = 2.8$ fm^{-1}. At higher q, the theoretical form factors begin to diverge from the data, particularly around the second diffraction minimum, which neither curve successfully replicates. The point at which the solid curve diverges from the dashed one, occurring at $q > 3$ fm^{-1}, marks the onset of the noticeable influence of correlation effects.

The longitudinal inelastic electron form factors for the ^{20}Ne and ^{24}Mg nuclei corresponding to the transitions $J_i^\pi T_i \rightarrow J_f^\pi T_f = (0^+0 \rightarrow 2^+0)$ and $(0^+0 \rightarrow 4^+0)$ are presented in Fig. 3—specifically, Fig. 3(a) for ^{20}Ne and Fig. 3(b) for ^{24}Mg—and in Fig. 4, with Fig. 4(a) and Fig. 4(b) displaying the respective results for ^{20}Ne and ^{24}Mg. To calculate the one-body density matrix (OBDM) elements required for transition densities and matrix elements in the inelastic electron scattering analysis, the OXBASH

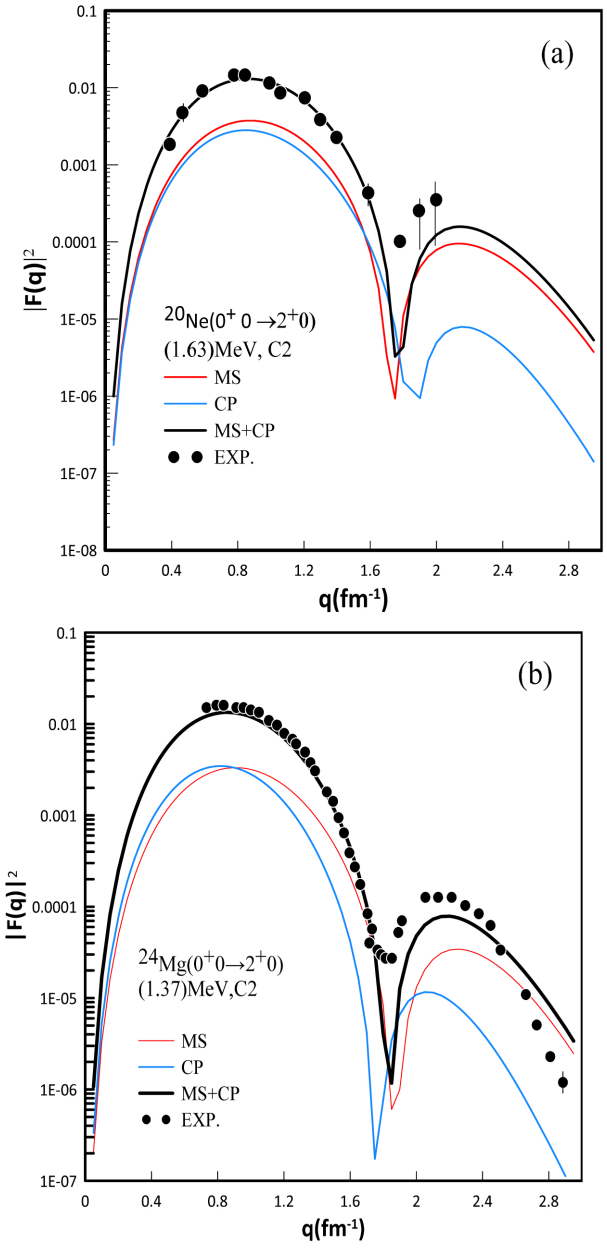

Fig. 3. The ^{20}Ne (Fig. a) and ^{24}Mg (Fig b) nuclei' inelastic longitudinal C2 form factors, which are compared with experimental data.

shell-model code was employed. OXBASH[21–23] code is a well-established nuclear structure code designed for performing large-scale shell-model calculations in various nuclear shells, including the sd-shell, which is relevant for the structure of ^{20}Ne and ^{24}Mg. The code allows configuration mixing, essential for accurate modeling of excited states and transition properties. In this study, the OBDMs obtained from OXBASH were used in conjunction with harmonic oscillator bases and the USDB (Universal sd-shell B) interaction, optimized for sd-shell nuclei. Parameters such as the oscillator size b were tuned to match experimental excitation energies. The usage of OXBASH ensures a reliable microscopic description of nuclear states, essential for reproducing longitudinal C2 and C4 form factors. The transition density in the model space is represented by Eq. (21). Core polarization effects were added via the Tassie model, as implemented in.[17] The excitation energy for ^{20}Ne is E_x = 1.63 MeV,[24] with an experimental value of $B(C2)$ = 278.3 e^2·fm^4;[25] for ^{24}Mg, E_x = 1.37 MeV,[22] with $B(C2)$ = 404.7 e^2·fm^4.[20] The red curves represent the model space contribution, which accounts for configuration mixing but excludes collective effects. In contrast, the blue curves represent the contribution from core polarization, which incorporates collective nuclear modes. The core polarization is modeled using the Tassie approach and is combined with the ground-state two-body charge density distributions (2BCDD's), calculated from Eq. (11). For illustration, the overall contribution—including both model space and core polarization effects—is represented by the black curves. The successful inclusion of core polarization is evidenced by the experimental results, shown as solid circles, which closely follow the black curves. The $C2$ form factor maxima in both the first and second transitions are enhanced by core polarization effects, which also produce calculated values that closely match the experimental data. The positions of the diffraction minima are shifted outward relative to those predicted by the pure *sd*-shell model (represented by the red lines). Additionally, the core polarization results exhibit a displacement toward smaller q values at higher momentum transfers, thereby improving the agreement between theoretical predictions and experimental measurements.

The longitudinal Coulomb C4 form factors calculated for ^{20}Ne and ^{24}Mg are presented as functions of the momentum transfer q for transitions corresponding to observed excitation energies of 4.25 MeV[26] (with an experimental value of $B(C4)$ = 32,500 e^2·fm^4)[21] for ^{20}Ne, and E_x = 6.1 MeV[20] (with B(C4) = 36,000 e^2·fm^4) for ^{24}Mg. As shown in Fig. 4—specifically, Fig. 4(a) for ^{20}Ne and Fig. 4(b) for ^{24}Mg—the red curves represent results from the mean-field structure (MS) with configuration mixing included, while the blue curves indicate the core polarization (CP) contribution when two-body correlations are accounted for. By including the effect of CP, the solid black curve—representing the total contribution—shows excellent agreement with experimental data. Furthermore, when CP effects are incorporated into the MS calculations, the results exhibit strong resonance with experimental data across the entire range of q.

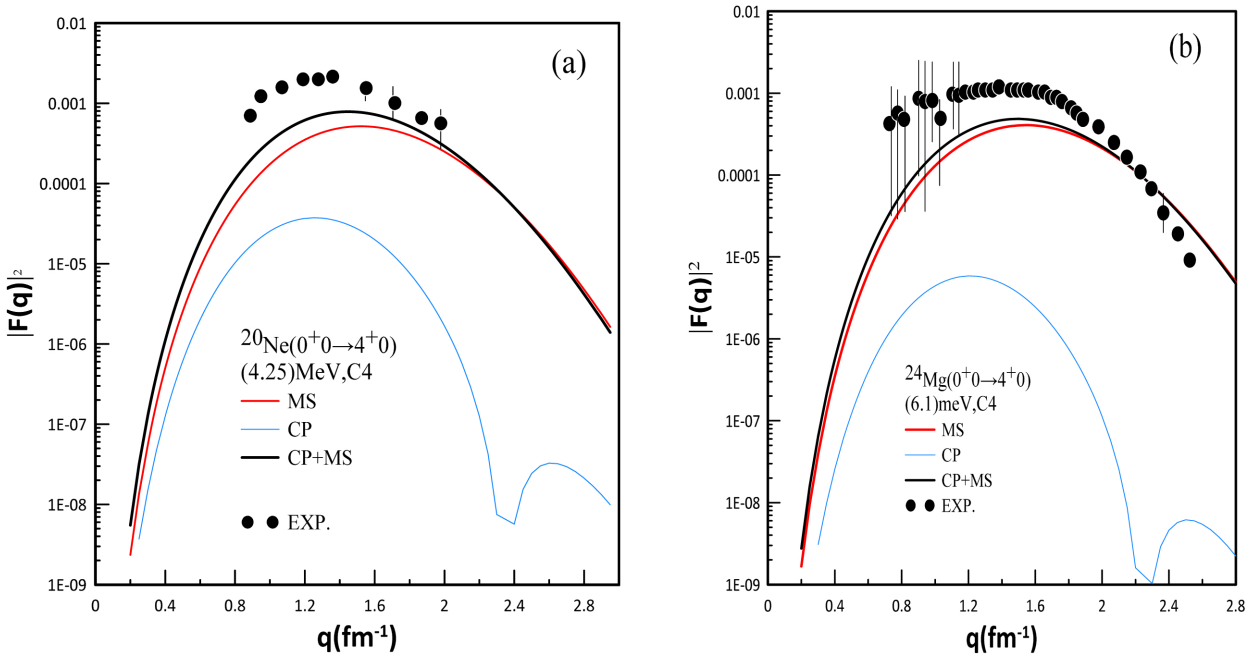

Fig. 4. Displays the ^{20}Ne (Fig. a) and ^{24}Mg (Fig b) nuclei' inelastic longitudinal C4 form factors.

Conclusions

The introduction of spin- and isospin-dependent interactions results in accurate predictions for the root-mean-square (RMS) charge radii of the ^{20}Ne and ^{24}Mg nuclei, as well as for their elastic electron scattering form factors. In particular, the application of the Tassie model for treating core polarization effects dramatically enhances the precision of inelastic form factor calculations for ground-state to excited-state transitions ($J_i^\pi T_i \rightarrow J_f^\pi T_f$), especially for $0^+ \rightarrow 2^+$ and $0^+ \rightarrow 4^+$ transitions. The results demonstrate the strength of the theoretical formalism in reproducing experimental data with very high accuracy, leading to improved physical insight into nuclear structure and a deeper understanding of the role that correlations play in determining nuclear properties. In summary, this work emphasizes the importance of precision in nuclear charge density distributions and electron scattering form factors when accounting for spin and isospin dependence, especially in relation to short-range correlations (SRC's). Through the use of an effective two-body density version of the folding model, the resulting charge density distributions accurately reflect these correlations.

Authors' declaration

- Conflicts of Interest: None.
- We hereby confirm that all the Figures and Tables in the manuscript are ours. Furthermore, any Figures and images that are not ours have been included with the necessary permission for republication, which is attached to the manuscript.
- No animal studies are present in the manuscript.
- No human studies are present in the manuscript.
- Ethical Clearance: The project was approved by the local ethical committee at the University of Baghdad.

Authors' contributions statement

F.F.K. developed the theoretical framework and performed calculations; G.N.F. conducted validation and analysis. Both authors contributed to writing and approved the final manuscript.

References

1. Ridha AR, Abbas ZM. Theoretical study of density distributions and size radii of ^{8}B and ^{17}Ne. Iraqi J Sci. 2018;59(2C):1046–1056. https://doi.org/10.24996/ijs.2018.59.2C.8.
2. Al-Rahmani AA, Fadhil SN, Hamoudi AK. Nuclear structure studies using relativistic mean-field theory. Iraqi J Sci. 2024;65(3):1357–68. https://doi.org/10.24996/ijs.2024.65.3.22.
3. Nguyen D, Novario SJ, Hergert H, Holt JD, Stroberg SR, Schwenk A. Ab initio calculations of medium-mass nuclei using the valence-space formulation. Phys Rev C. 2023;108(2):024305. https://doi.org/10.1103/PhysRevC.108.024305.
4. Weiss R, Lovato A, Hergert H, Piarulli M, Wiringa RB, Pieper SC. Nuclear charge radii and neutron skins from chiral

effective field theory. Phys Rev D. 2022;106(5):056016. https://doi.org/10.1103/PhysRevD.106.056016.
5. Cruz-Torres R, Schmidt A, Miller GA, Weinstein LB, Barnea N, Weiss R, Piasetzky E, Hen O. Short-range correlations and the isospin dependence of nuclear correlation functions. Phys Rev C. 2021;103(5):054603. https://doi.org/10.1103/PhysRevC.103.054603.
6. Weiss R, Schmidt A, Miller GA, Barnea N. Shortrange correlations and the charge density. Phys Lett B. 2019;790:484–489. https://doi.org/10.1016/j.physletb.2019.01.053.
7. Hamoudi AK, and Abbas MA. Electron scattering from some even fp- and N50-shell nuclei with implanting the influence of short-range correlation functions. Chin. J. Phys. 2019;60:623–631. https://doi.org/10.1016/j.cjph.
8. Flaiyh GN, Sharrad FI. Inelastic longitudinal C2 form factors with corepolarization effects for ^{10}B nucleus. Iran J Sci Technol Trans A Sci. 2018;42(4):2323–2328. https://doi.org/10.1007/s409950170160X.
9. Sharp P, Schmidt A. Observing shortrange correlations in nuclei through ρ^0 photoproduction. Eur Phys J A. 2025;61(2):40. https://doi.org/10.1140/epja/s10050-025-01505-9.
10. Ye Z, SolvignonSlifer P, Nguyen D, Arrington J, Fomin N, Meziani ZE, et al. Measurement of the EMC effect in light nuclei. Phys Rev Lett. 2023;128(13):132501. https://doi.org/10.1103/PhysRevLett.128.132501.
11. Khalil I, Abdalsada A, Al-Rahmani AA. Inelastic form factors for the ^{90}Zr nucleus with short-range correlations effect. Iraqi J Sci. 2024;65(12):7005–20. https://doi.org/10.24996/ijs.2024.65.12.17.
12. Fiase JO, Hamoudi A, Irvine JM, Yazici F. Effective interactions for sdshell model calculations. J Phys G: Nucl Part Phys. 1988;14:27–49. https://doi.org/10.1088/0305-4616/14/1/007.
13. Heyde KLG, Wood JL. The nuclear shell model: recent developments and perspectives. Prog Part Nucl Phys. 2021;118:103855. https://doi.org/10.1016/j.ppnp.2021.103855.
14. Jassim KS, Sahib SR. Largescale shell model calculations of the ^{25,26}Mg, ^{27}Al and ^{19}F nucleus. Int J Nuclear Energy Sci Technol. 2018;12(1):81–91. https://doi.org/10.1504/IJNEST.2018.092601.
15. Brown BA, Lisetskiy AF, Horoi M, Schultz B, Whitehead M, McGrory J, *et al.* Advances in shell-model calculations for nuclear excitations. Prog Part Nucl Phys. 2021;118:103855. https://doi.org/10.1016/j.ppnp.2021.103855.
16. Bertulani CA, AbdulKhalek R, Accardi A, Anderle D, Aschenauer EC, Bacchetta A, *et al.* Electron-Ion Collider and the science of nuclear femtography. Prog Part Nucl Phys. 2022;127:103983. https://doi.org/10.1016/j.ppnp.2022.103983.
17. Abbas ZM, Flaiyh GN. Study of charge density distributions, elastic and inelastic electron scattering form factors and size radii for ^{24}Mg and ^{28}Si nuclei. Al-Nahrain J Sci. 2025;28(4):76–82.
18. de Vries H, de Jager CW, de Vries C. Nuclear charge and magnetization density distribution parameters. At Data Nucl Data Tables. 1987;36(3):495–566. https://doi.org/10.1016/0092-640X(87)90013-1.
19. Fricke G, Heilig K, Schopper H, Anton J, Baumann P, Bollen G, *et al.* Nuclear ground state charge radii from elastic electron scattering. At Data Nucl Data Tables. 1995;60(2):177–285. https://doi.org/10.1006/adnd.1995.1007.
20. Li GC, Yearian MR, Sick I. Highmomentumtransfer electron scattering from ^{24}Mg, ^{27}Al, ^{28}Si and ^{32}S. Phys Rev C. 1974;9:1861–1877. https://doi.org/10.1103/PhysRevC.9.1861.
21. Amos K, Steward C. Large basis space effects in electron scattering form factors of light nuclei. Phys Rev C. 1990;41:335–341. https://doi.org/10.1103/PhysRevC.41.335.
22. Brown BA, Rae WDM, Horoi M, Signoracci A, Stroberg SR, Schwenk A, Vary JP. NuShellX 2023: advanced shell-model calculations. Comput Phys Commun. 2023;292:108870. https://doi.org/10.1016/j.cpc.2023.108870.
23. Hameed BS, Rejah BK. Study the nuclear structure of some cobalt isotopes. Baghdad Sci J. 2022;19(6):1566–1571. https://doi.org/10.21123/bsj.2022.7537.
24. Tichai A, Ripoche J, Duguet T, Morris TD, Stroberg SR, Holt JD, Schwenk A. Ab initio shell model for medium-mass nuclei. Phys Rev C. 2023;108(3):034310. https://doi.org/10.1103/PhysRevC.108.034310.
25. Knight EA, Singhal RP, Macauley MW. Elastic scattering of electrons from ^{20}Ne. J Phys G Nucl Phys. 1981;7(8):1115–26. https://doi.org/10.1088/0305-4616/7/8/018.
26. Koning AJ, Rochman D, Sublet JC, Dzysiuk N, Fleming M, Van Der Marck SC. Global optical potential for nucleon-nucleus scattering. Phys Rev C. 2023;108(5):054602. https://doi.org/10.1103/PhysRevC.108.054602.

دراسة تأثير الارتباطات قصيرة المدى والاعتماد الأيزوسبيني لدوال الارتباط النووي باستخدام صيغة التلامس

فرح فارس قدوري[1،2]، غيث نعمه فليح [1]

[1] قسم الفيزياء، كلية العلوم، جامعة بغداد، بغداد، العراق.
[2] قسم الفيزياء، كلية العلوم للبنات، جامعة بغداد، بغداد، العراق.

الخلاصة

تمثل كثافات الأزواج ودوال الارتباط المرتبطة بها أدوات أساسية لدمج تأثيرات الأجسام المتعددة في النظريات النووية. تبحث هذه الدراسة التأثيرات المباشرة للاعتماد على spin وisospin في توزيعات كثافة الشحنة النووية. باستخدام folding model تم حساب توزيع كثافة الشحنة مع مراعاة كل من الارتباطات قصيرة المدى (SRC) وارتباطات tensor ، من خلال صيغة فعالة لكثافة الجسمين تأخذ في الاعتبار تفاعلات spinوisospin . شملت الحسابات عوامل شكل التشتت الإلكتروني المرن F(q) ونصف قطر جذر متوسط الشحنة التربيعي ($\langle r^2\rangle^{1/2}$) لنواتي 20Ne و24Mg ، بالإضافة إلى عوامل التشكل للاستطارة الطولية الغير مرنة للانتقالات النووية المتساوية القياس (T=0) من (0^+ → 0^+) و (0^+ → 4^+) ، مع تضمين تأثيرات استقطاب النواة باستخدام انموذج Tassie. أظهرت النتائج توافقاً جيداً مع البيانات التجريبية، مما يؤكد دقة ومتانة الإطار النظري المعتمد.

الكلمات المفتاحية: توزيع كثافة الشحنة (CDD)، تأثيرات استقطاب النواة، عامل الشكل (FF)، الارتباط قصير المدى (SR’C)، ارتباطات الموتر (TC’s).